Development 135, 33-41 (2008) doi:10.1242/dev.010892

chongmague reveals an essential role for laminin-mediated boundary formation in chordate convergence and extension movements

Michael T. Veeman, Yuki Nakatani*, Carolyn Hendrickson, Vivian Ericson, Clarissa Lin and William C. Smith†

Although cell intercalation driven by non-canonical Wnt/planar cell polarity (PCP) pathway-dependent mediolateral cell polarity is important for notochord morphogenesis, it is likely that multiple mechanisms shape the notochord as it converges and extends. Here we show that the recessive short-tailed *Ciona savignyi* mutation *chongmague* (*chm*) has a novel defect in the formation of a morphological boundary around the developing notochord. *chm* notochord cells initiate intercalation normally, but then fail to maintain their polarized cell morphology and migrate inappropriately to become dispersed in the larval tail. This is unlike *aimless* (*aim*), a mutation in the PCP pathway component Prickle, which has a severe defect in early mediolateral intercalation but forms a robust notochord boundary. Positional cloning identifies *chm* as a mutation in the *C. savignyi* ortholog of the vertebrate alpha 3/4/5 family of laminins. *Cs*-lamα3/4/5 is highly expressed in the developing notochord, and *Cs*-lamα3/4/5 protein is specifically localized to the outer border of the notochord. Notochord convergence and extension, reduced but not absent in both *chm* and *aim*, are essentially abolished in the *aim*/*aim*; *chm*/*chm* double mutant, indicating that laminin-mediated boundary formation and PCP-dependent mediolateral intercalation are each able to drive a remarkable degree of tail morphogenesis in the absence of the other. These mechanisms therefore initially act in parallel, but we also find that PCP signaling has an important later role in maintaining the perinotochordal/intranotochordal polarity of *Cs*-lamα3/4/5 localization.

KEY WORDS: *Ciona*, Morphogenesis, Notochord, Planar cell polarity

INTRODUCTION

Convergence and extension (CE) movements shape chordate embryos such that they become longer along the anteroposterior axis and narrower across the mediolateral axis (Keller, 2002; Wallingford et al., 2002). In vertebrates, CE movements are most pronounced in the tissues that form the notochord, somites and spinal cord. These movements have been best characterized in explanted *Xenopus* dorsal mesoderm, where they include cell intercalation driven by mediolaterally-biased tractive cell protrusions as well as 'boundary capture', the tendency of cells to become quiescent on surfaces contacting the nascent notochord/somite boundary (Keller et al., 1989; Shih and Keller, 1992a). Planar cell polarity (PCP) signaling is known to be a key mediator of mediolateral intercalation and related cell behaviors (Veeman et al., 2003; Wang and Nathans, 2007). The molecular basis of morphogenetic behaviors at the notochord boundary are much less well understood, although components of the extracellular matrix and integrins have been implicated in directing both motility and boundary behavior (Marsden and DeSimone, 2003; Davidson et al., 2006).

We use the ascidian *Ciona savignyi* as a model for chordate axial morphogenesis, both for the morphological simplicity of its body plan and the genetic simplicity of its compact genome. Ascidian notochord morphogenesis takes place without cell division and involves the intercalation of only 40 notochord cells from an initially isodiametric grouping into a single-file column of flat, disk-shaped cells (Cloney, 1964; Miyamoto and Crowther, 1985; Munro et al., 2006; Munro and Odell, 2002b). This intercalation involves mediolaterally-biased tractive cell protrusions, as has also been described in *Xenopus* (Shih and Keller, 1992a; Shih and Keller, 1992b), and may involve a ventrally oriented invagination movement that helps round the notochord in cross section (Munro and Odell, 2002b). While this intercalation is essential, a considerable degree of tail extension is also driven by cell-shape changes and vacuolization after intercalation is complete (Miyamoto and Crowther, 1985). Although notochord intercalation appears broadly similar between ascidians and vertebrates, there are likely to be important differences between ascidian and vertebrate CE movements. For example, ascidian muscle and neural cells do not obviously play as active and independent a role in CE as they do in vertebrates.

The *Ciona* mutation *aimless* (*aim*) is an allele of the PCP pathway component Prickle (Pk) (Jiang et al., 2005). *aim* notochord cells have severe defects in mediolateral cell polarity and, although fully motile, they converge and extend extremely slowly and incompletely, such that most of the notochord remains roughly two cells wide. The notochord-specific RNA expression (Hotta et al., 2000; Jiang et al., 2005) and mutant phenotype of *aim* suggest that the ascidian PCP pathway is involved only in notochord morphogenesis and not in gastrulation or neural tube closure. Although *aim* is probably a null mutation and has a severe defect in notochord cell behavior, the notochord cells do form a rod-like structure and the tail does show considerable elongation. These observations suggest that multiple mechanisms are important in the overall convergence and extension of the ascidian tail.

A second mutation, *chongmague* (*chm*), causes a distinct and profound defect in notochord morphogenesis. All 40 notochord cells are present and express notochord-specific genes such as *brachyury* (*bra*), *forkhead* and *tropomyosin* (Deschet et al., 2003;

Department of Molecular, Cell and Developmental Biology, University of California Santa Barbara, Santa Barbara CA, 93106, USA.

*Present address: Department of Biology, Ochanomizu University, 2-1-1 Otsuka, Bunkyo-ku, Tokyo 112-8610, Japan
†Author for correspondence (e-mail: w_smith@lifesci.ucsb.edu)

Accepted 30 September 2007

Nakatani et al., 1999), but the notochord cells appear rounded and fail to adopt the wild-type 1×40 'stack of coins' morphology. Markers for other embryonic tissues, including tail muscle, nervous system and epidermis, are correctly expressed within the context of a short and aberrant tail (Deschet et al., 2003; Nakatani et al., 1999). Here we use high-resolution 3D confocal imaging to show that *chm* has a novel and severe defect in the formation of a morphological boundary around the developing notochord. Unlike in *aim*, early intercalation is relatively normal, but the notochord cells lose their polarized morphology and become widely dispersed in the tail.

We hypothesized that the dispersed notochord cells seen in *chm* reflect a failure in boundary capture or some similar behavior at the notochord border. Wild-type ascidian embryos exhibit a suite of complex behaviors at the notochord border, including a surprisingly dynamic boundary capture-like behavior in which notochord cells rapidly spread out on surfaces contacting the boundary. *chm* notochord cells show persistent and undirected motility that is consistent with a failure in this behavior. We have identified *chm* as a mutation in *Cs*-lamα3/4/5, an extracellular matrix (ECM) molecule highly expressed in the notochord and specifically localized to perinotochordal cell surfaces.

Although the notochord boundary can be perturbed by genetic manipulations that transform notochord cells into muscle and vice-versa (Fujiwara et al., 1998; Reintsch et al., 2005), *chm* is, to the best of our knowledge, the only perturbation with a strong, early and direct effect on the formation of the notochord boundary. *chm* thus provides a unique tool to functionally test the relationship between notochord boundary formation and PCP-dependent cell intercalation. Epistasis analysis suggests that these two mechanisms initially act largely in parallel. The considerable convergence and extension remaining in *aim* is dependent on *chm* function, suggesting that the notochord boundary does not merely support the structural integrity of the notochord and help maintain polarized cell behaviors, but that it can itself drive a significant amount of CE. The relationship between PCP signaling and laminin-mediated boundary formation is not strictly independent, however, as we also observe that the PCP pathway has a role in maintaining the perinotochordal/intranotochordal polarity of *Cs*-lamα3/4/5 localization.

MATERIALS AND METHODS

Ascidian culture and genetics

Mutant ascidian lines were cultured in a running seawater facility as described (Hendrickson et al., 2004). *Ascidiella aspers*a were obtained from the Woods Hole Marine Biological Laboratory. The experiments using the *bra:GFP* transgene used the chm^{35} allele of *chm*, otherwise all experiments used the original *chm* allele.

Antibody and phalloidin staining

Embryos were fixed in either 2% paraformaldehyde in seawater or Munro's Ascidian Cytoskeletal Fix (2% paraformaldehyde, 0.1 M Hepes pH 7.0, 0.05 M EGTA, 0.4 M dextrose, 0.01 M $MgSO_4$, 0.2% Triton X-100), rinsed several times in PBT (PBS+0.2% Triton-X) and fixed in 5% heat-inactivated goat serum in PBT. Bodipy-FL phallacidin (Invitrogen) was used at 1 unit/100 μl, anti*Cs*-lamα3/4/5 at 1:250-1:500, rabbit polyclonal anti-GFP at 1:500 and mouse monoclonal anti-GFP at 1:250. The *Cs*-lamα3/4/5 antibody was raised against a bacterially produced recombinant protein containing amino acids 1330 to 1494 of *Cs*-lamα3/4/5(lam13) fused to an N-terminal His tag. *Cs*-lamα3/4/5 staining required an antigen retrieval step (Kirkpatrick and d'Ardenne, 1984) with 20-40 μg/ml proteinase K in PBT for 4 minutes at 37°C followed by several brief washes in PBT on ice. Primary and secondary antibody incubations were overnight at 4°C, followed by several washes in PBT. Bodipy-FL phallacidin was used for 1 hour at room temperature in PBT, followed by several washes in PBT. Two-color GFP/phalloidin staining used a rabbit polyclonal anti-GFP antibody and a red fluorescent Alexa 594 secondary antibody to detect GFP in combination with the green fluorescent Bodipy-FL phallicidin (direct GFP fluorescence is killed by the clearing process). Embryos were cleared and mounted as described (Munro and Odell, 2002b). Electroporations were as described (Corbo et al., 1997).

Imaging

An Olympus Fluoview 500 was used for confocal imaging, using 40× 1.2NA and 60× 1.4NA oil immersion lenses for fixed samples and a 20× 0.7NA air lens for live imaging. Image stacks were at 0.4-0.5 μm spacing for fixed embryos. ImageJ (Wayne Rasband, NIH) was used to reconstruct *z*-sections across the axis of the notochord, and for maximum intensity projections. Slidebook 4.1 (Intelligent Imaging Innovations) was used for volume renderings of confocal stacks. Widefield images were collected using a Leica DMRB compound microscope with a shutter-controlled epifluorescence light path and either a SPOT-2 or a Hamamatsu ERAG CCD camera.

Mapping the *chm* mutation

Bulked segregant analysis (BSA) was performed on DNA isolated from triplicate pools of 15 embryos each from mutant (*chm*/*chm*) and phenotypically wild-type (wt/wt and wt/*chm*) progeny of a self-fertilized heterozygous *chm* adult, as described previously (Jiang et al., 2005). AFLP reactions on the pooled genomic DNAs were performed using the Small Genome Kit from Invitrogen. The AFLP reactions were resolved on sequencing gels and autoradiographed. Linked bands were eluted from the gels, reamplified, and sequenced using standard fluorescent sequencing methods. Nucleotide sequences of the linked bands were used to search the partially assembled *C. savignyi* genomic sequence.

Cs-lamα3/4/5 nucleotide sequence analysis

Cs-lamα3/4/5 genomic sequences predicted by paired scaffolds 312 and 44 were used to search protein and nucleic acid databases, including the *C. intestinalis* EST database (Imai et al., 2004). We were able to identify with high confidence N- and C-terminal ESTs for the *C. intestinalis* ortholog of *Cs*-Lamα3/4/5. These *C. intestinalis* EST sequences were then used as guides with the *C. savignyi* genomic sequence to design oligonucleotides to the 5′ and 3′ ends of the *Cs*-Lamα3/4/5 transcript (GAAATATTAGA-GTCGCAAAAAACTAGTCAATGACC and GGTCTATGGCGATATT-ACGACAAATAACTGTCC, respectively).

The oligonucleotides were used to amplify an ~11 kbp PCR product using LaTaq (Takara) with cDNA synthesized from RNA extracted from pooled clutches of wild-type *C. savignyi* larvae. Two separate alleles of the wild-type *Cs*-lamα3/4/5 cDNA clones of 11,354 bp (clone *lam13*) and 11,605 bp (clone *lam33*) were sequenced in their entirety, and two conceptual cDNAs were derived from the *C. savignyi* genomic sequence (*haplo1* and *haplo2*). *Cs*-lamα3/4/5 cDNAs from pools of homozygous *chm* and chm^{35} larvae were PCR-amplified in three overlapping fragments. Genomic fragments containing the frameshift mutation identified in the chm^{35} cDNA were PCR-amplified from individual larvae using the oligonucleotides 5′-GGA-AATGTGCAACCACACG-3′ and 5′-TCTGTTCTTAAGGTCATTGG-CAT-3′ and directly sequenced.

Cs-lamα3/4/5 in situ hybridization

For late-tailbud-stage embryos, in situ hybridization was as described (Arenas-Mena et al., 2000), using a 986 bp internal cDNA fragment from base 4427 to base 5413 of the lam13 cDNA. For neurula-stage embryos, a 2032 bp probe from the 3′ end of the full-length transcript was used as described (Hotta et al., 1999).

Morpholino oligonucleotide knockdown

Fertilized eggs were injected with either sense or anti-sense morpholino oligonucleotides (MOs) corresponding to the predicted start codon and flanking 3′ nucleotides of the *Cs*-lamα3/4/5 gene (sense: TCAATGA-CCAAAATGCTGCGCTTAG; antisense: CTAAGCGCAGCATTTTGG-TCATTGA). Eggs were injected with ~15 pl MO solutions at 0.5 or 0.67 mM (final dose ~10 fmol), as described previously (Imai et al., 2002).

Single tadpole DNA prep

Tadpole larvae were fixed in 3.7% formaldehyde in seawater. After several days in fixative, the test cells sloughed off, thus removing any potential maternal DNA contamination. The larvae were then rinsed in distilled water and transferred individually to tubes containing 10 μl of 1% Triton X-100, 100 mM NaCl, 20 mM Tris pH 7.8, 1 mM EDT, and 1 mg/ml proteinase K. The samples were incubated overnight at 55°C, followed by a 10 minute incubation at 95°C to inactivate the protease.

RESULTS

Early intercalation in *chm* is relatively normal, but the notochord cells fail to maintain polarized cell shapes

Confocal microscopy of a notochord-specific *brachyury:GFP* (*bra:GFP*) transgene (Deschet et al., 2003) in fixed and cleared embryos allows high-resolution analysis of notochord morphogenesis. Although *chm* and *aim* are superficially similar in that both have short tails, the underlying phenotypes are distinct at the cellular level. At early tailbud stage, the earliest stage when *chm* can be identified, considerable convergence and extension had already occurred and the *chm* notochord was only slightly shorter and wider than wild-type (Fig. 1A,B). Identically staged *aim* embryos had undergone little convergence and extension and thus had much shorter, wider notochords (Fig. 1C). *aim* embryos also manifest their mutant phenotype considerably earlier (Jiang et al., 2005) (and data not shown). Unlike in wild-type and *aim* embryos, however, the *chm* notochord had an irregular outer border, with many lateral cells elongated along the anteroposterior axis instead of the mediolateral axis (green arrowheads in Fig. 1B).

By mid-tailbud stage, the wild-type notochord has fully intercalated into a compact rod of 40 disk-shaped cells (Fig. 1D,F). In *chm*, however, notochord morphology had become completely aberrant, with rounded, loosely adherent cells forming a dispersed mass in the tail (Fig. 1E,G,H,I). The wild-type notochord is located centrally in the tail, flanked by the dorsal nerve cord, the ventral endodermal strand and the lateral muscle cells (inset in Fig. 1F). In *chm*, however, notochord cells could be found invading these flanking tissues, most frequently the nerve cord (Fig. 1H) and endodermal strand (Fig. 1I), and occasionally the muscle cells. For rotating 3D renderings of these confocal stacks, see Movies 1 and 2 in the supplementary material. *chm* embryos also showed a characteristic epidermal protrusion at the tip of the tail (yellow bracket in Fig. 1E and see Movie 3 in the supplementary material).

Ascidian embryos exhibit complex and dynamic behaviors at the notochord boundary

The failure of *chm* notochord cells to either form or respect a morphological boundary between themselves and the flanking tissues is reminiscent of the process of boundary capture that has been described in *Xenopus* embryos, whereby intercalating axial and paraxial mesodermal cells become quiescent on surfaces contacting the nascent notochord/somite boundary (Keller et al., 1989; Shih and Keller, 1992a; Wallingford et al., 2002). Although time-lapse studies of ascidian notochord morphogenesis have been reported, none have focused on the morphogenetic processes at the notochord boundary (Miyamoto and Crowther, 1985; Munro and Odell, 2002b). To better characterize these processes in wild-type ascidians, we made use of the strikingly transparent embryos of *Ascidiella aspersa* (Berrill, 1930), which allow much higher quality DIC imaging than in *Ciona* (see Movie 4 in the supplementary material).

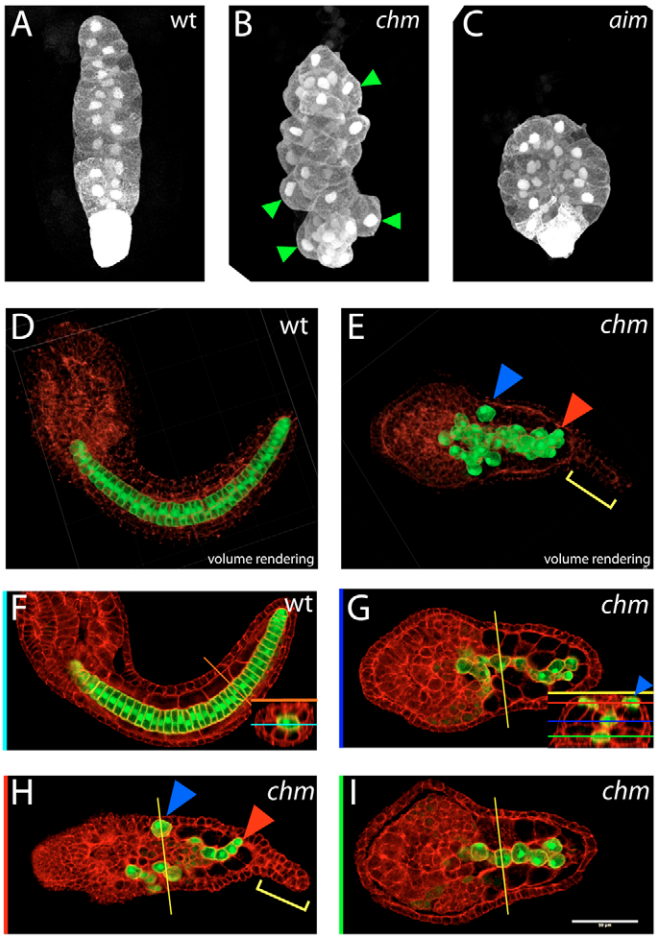

Fig. 1. Notochord morphology in *chongmague*. All images show the notochord-specific *bra:GFP* transgene (white in A-C, green in D-I). Although not fused to any localization signal, the GFP is consistently brighter in the nucleus and cell cortex, and also brighter in the eight secondary lineage notochord cells at the posterior tip of the tail. Panels D-I also show the actin cytoskeleton labeled with phallacidin in red. (**A-C**) Maximum intensity projections of confocal stacks through identically staged wild-type (A), *chm/chm* (B) and *aim/aim* (C) embryos. Anterior to the top. Green arrowheads in B show notochord cells at the edges of the notochord that have their long axes inappropriately oriented along the anteroposterior and not the mediolateral axis. (**D**,**F**) Mid-tailbud-stage wild-type embryo. Anterior is to the left. (D) A volume rendering of the entire confocal stack and (F) a single slice at the level indicated by the blue line (inset). The inset shows a cross section along the orange line in the main panel. (**E**,**G-I**) *chm/chm* sibling. Anterior is to the left. (E) A volume rendering and (G-I) single slices at the levels indicated on the cross-section inset in G as indicated by the coloured lines to the left of each panel. The blue arrowheads mark an isolated notochord cell at the periphery of the tail. The red arrowhead marks a notochord cell interdigitated between two muscle cells. The yellow bracket marks the characteristic epidermal protrusion at the tip of the *chm* tail. Scale bar: 50 μm.

At the beginning of intercalation, the notochord primordium was difficult to distinguish from the surrounding cells, but as intercalation proceeded it became increasingly distinct (Fig. 2A). This is largely a result of the notochord cells each forming a neat, flat edge with the flanking muscle cells. Tracking of individual notochord cells revealed that they did not simply become quiescent on surfaces contacting the boundary, but that they actively and

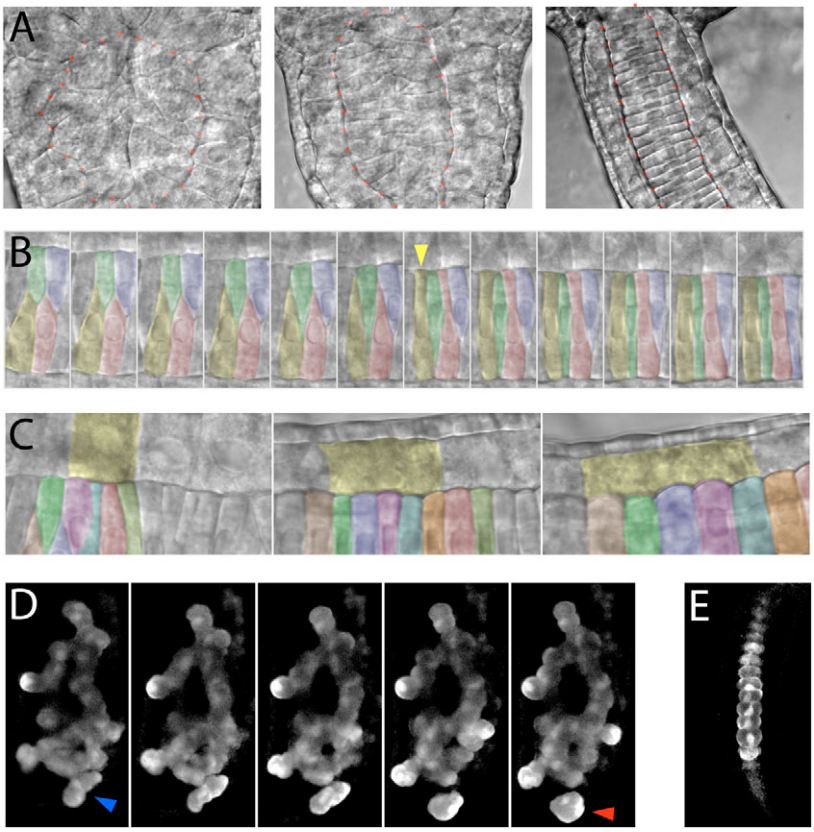

Fig. 2. Time-lapse analysis of ascidian notochord boundary formation. (**A-C**) Nomarski time-lapses of notochord boundary formation in the highly transparent ascidian *Ascidiella aspersa*. (A) Emergence of a morphologically distinct notochord boundary (marked with orange dots). Frames are 100 minutes apart. (B) Cell behaviors at the notochord boundary late in intercalation. Note the rapid spreading of the yellow cell as it contacts the boundary (indicated by the yellow arrowhead), while the adjacent green cell becomes temporarily displaced. Frames are 3 minutes apart. (C) Gradual shearing of muscle cells (one marked in yellow) versus notochord cells along the notochord boundary. Frames are 75 minutes apart. (**D**) Confocal time-lapse of *bra:GFP* fluorescence in a *chm/chm Ciona savignyi* embryo. Anterior is to the top. Note the small group of cells in the first frame (blue arrow) that break away from the main mass of the notochord and migrate toward the tip of the tail (red arrow in the final frame). There is also considerable movement of cells at the notochord boundary, especially on the bottom right side of the image. Frames shown are 16 minutes apart. (**E**) A single frame of *bra:GFP* fluorescence in a wild-type sibling imaged just after the time-lapse in D was completed.

rapidly spread out as they made contact (e.g. the yellow cell as it approached and contacted the boundary in Fig. 2B). A cell newly contacting the boundary often partially displaced its neighbors before they re-established an equilibrium of boundary contact (e.g. the green cell displaced its yellow neighbor on contact with the boundary in Fig. 2B). We also note that notochord cell nuclei became polarized away from the notochord boundary (Fig. 2B).

Although this rapid spreading and flattening as notochord cells contact the boundary is suggestive of an adhesive process, the notochord boundary acts as more than simply a substrate for cell adhesion. By tracking the relative positions of notochord and muscle cells over time, it was clear that there is shearing or sliding of cells along this interface (Fig. 2C). Such shearing implies that there must be some active process at work to account for the simultaneous adhesion and movement of cells along the boundary.

We also observed rhythmic pulsatile behaviors at the lateral edges of the notochord cells that persisted long after intercalation (see Movie 4 in the supplementary material). Miyamoto and Crowther observed a similar behavior in *Ciona*, which they suggested might be a form of blebbing involved in secreting the perinotochordal basement membrane (Miyamoto and Crowther, 1985). In our high-resolution recordings, these pulsatile movements did not appear to be blebbiform in nature, and we hypothesize that they may be involved in breaking and reforming adhesions as the boundary remodels itself during post-intercalation tail extension.

chm shows persistent notochord cell motility

Although *Ciona* is not as well suited to live imaging as *Ascidiella*, we were previously able to use time-lapse microscopy of the *bra:GFP* transgene to show persistent notochord cell motility in *chm* (Deschet et al., 2003) (see Movie 5 in the supplementary material). Those wide-field images were unable, however, to resolve individual notochord cells. Here we used confocal microscopy to image GFP-expressing *chm* notochord cells as they migrated to the periphery of the tail (see Movie 6 in the supplementary material). In the time-lapse sequence shown in Fig. 2D, one small group of cells that was initially contiguous with the main mass of the notochord (blue arrowhead) broke away and migrated toward the tip of the tail (red arrowhead). These cells showed rapid and largely undirected lamelliform protrusions that were absent at this stage in the notochord cells of wild-type siblings (Fig. 2E).

chm is *Cs*-lamα3/4/5

The aberrant cell morphology and movement of the *chm* notochord cells suggests two main hypotheses: *chm* might represent a defect in adhesion between notochord cells or it might reflect a failure to form a basement membrane or other barrier between the notochord and flanking tissues. To distinguish between these and other possibilities, we used amplified fragment length polymorphism analysis on bulked pools of segregants (AFLP-BSA) to map *chm*, initially finding two potentially linked markers on paired scaffold 44 (now part of reftig 96) and one on paired scaffold 312 (now part of reftig 19) of the partially assembled *C. savignyi* genome (Fig. 3A). An examination of potential open reading frames revealed that these two genomic scaffolds encoded the C- and N-terminal regions, respectively, of a predicted alpha laminin gene. An alpha laminin cDNA that spans these two scaffolds confirmed that they were contiguous. Single-strand confirmation polymorphism (SSCP) confirmed tight genetic linkage at the alpha laminin locus (SSCP2; Fig. 3A) and partial linkage near the most distant AFLP marker (SSCP1; Fig. 3A).

Laminins are polymeric heterotrimers of large alpha, beta and gamma chains that are important components of the basement membranes (basal laminae) that serve to adhere cells and separate tissues (Sasaki et al., 2004). Given that *chm* is defective in forming a

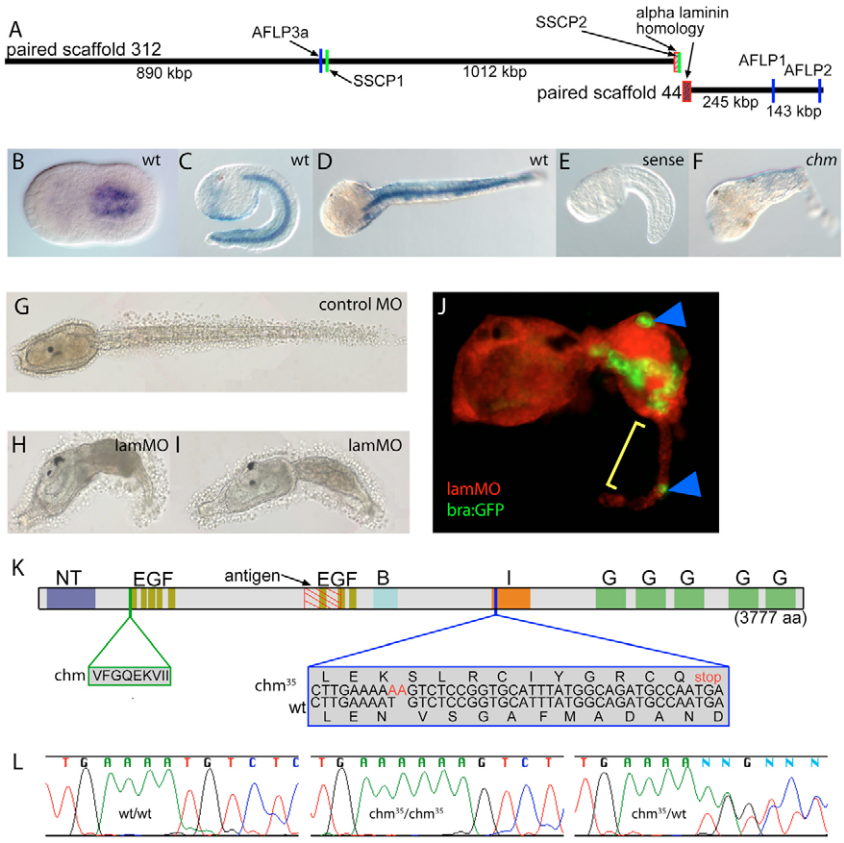

Fig. 3. *Chm* is *Cs*-lamα3/4/5. (**A**) Schematic of AFLP and SSCP mapping showing a predicted alpha laminin gene on paired scaffolds 312 and 44 in *C. savignyi*. (**B-D**) Whole-mount in situ hybridization for *Cs*-lamα3/4/5 message showing notochord-specific expression in (B) late neurula, (C) mid-tailbud and (D) late tail extension stages. (**E**) Sense control and (**F**) decreased expression in a *chm/chm* embryo. (**G**) Embryo injected with control morpholino. (**H**,**I**) *Cs*-lamα3/4/5 morphant embryos showing the range of phenotypes observed. (**J**) *bra:GFP* expressing embryo co-injected with *Cs*-lamα3/4/5 morpholino and red fluorescent dextran as an injection marker. Note the disorganized notochord boundary, the dispersed *bra:GFP*-expressing cells in the tail (blue arrowheads) and the characteristic epidermal protrusion (yellow bracket). (**K**) Schematic of *Cs*-lamα3/4/5 domain structure showing a 9 amino acid insertion in *chm* and a frameshift predicted to cause to premature termination in chm^{35}. The antigen used to make the *Cs*-lamα3/4/5 antibody is indicated. (**L**) Chromatograms showing the chm^{35} frameshift in genomic DNA from wt/wt, chm^{35}/ chm^{35} and chm^{35}/wt individuals. wt, wild type.

morphological boundary between the notochord and its flanking tissues, a basement membrane component such as a laminin was a strong candidate gene. A phylogenetic analysis revealed that this gene was one of only two *C. savignyi* alpha laminins, and was most closely related to vertebrate alpha 3, 4 and 5 laminins (see Fig. S1 in the supplementary material). Accordingly, we named it *Cs*-lamα3/4/5.

In situ hybridization against *Cs*-lamα3/4/5 message showed that it was strongly expressed in the notochord during tail extension (Fig. 3B,C,D). There was also faint expression throughout the tail and the epidermis at later stages. In *chm*, *Cs*-lamα3/4/5 RNA expression was greatly reduced and the strong notochord-specific expression was eliminated (Fig. 3F). Both the strong notochordal expression and the decreased expression in *chm* mutant embryos are consistent with *Cs*-lamα3/4/5 being *chm*.

To further investigate *Cs*-lamα3/4/5 as a candidate for *chm*, fertilized eggs were injected with either sense or antisense MOs corresponding to the predicted start codon and adjacent 3′ nucleotides of *Cs*-lamα3/4/5. The majority of embryos injected with the antisense MO showed a short tail and epidermal protrusion phenotype characteristic of *chm* [74% (*n*=23) and 83% (*n*=24), for two independent experiments]. The two larvae presented in Fig. 3H,I show the range of phenotypes observed, which closely mirrored the range of phenotypes seen in *chm*/*chm* embryos. By contrast, none of the embryos injected with the control sense MO showed this *chm*-like phenotype (*n*=62 and 99, for the two experiments, and Fig. 3G). To further examine the morphant phenotype, we also injected the *Cs*-lamα3/4/5 antisense morpholino into eggs fertilized with sperm carrying the *bra:GFP* transgene. This revealed an irregular notochord boundary with notochord cells widely dispersed in the tail (Fig. 3J), exactly as seen in the *chm* mutant (Fig. 1E). Other aspects of *chm* were also closely phenocopied, including the formation of a long epidermal protrusion at the tip of the tail.

Sequencing of *Cs*-lamα3/4/5 cDNAs from *chm* and two wild-type alleles revealed multiple non-synonymous polymorphisms, and a splicing variation found only in *chm* that created a 9 amino acid insertion (Fig. 3K). A second non-complementing allele, chm^{35}, was isolated in a screen for spontaneous mutations in the wild *C. savignyi* population (Hendrickson et al., 2004). chm^{35} was phenotypically indistinguishable from *chm*, and also showed tight genetic linkage to Cs-lamα3/4/5 (see Fig. S2 in the supplementary material). Nucleotide sequence analysis of *Cs*-lamα3/4/5 cDNA and genomic DNA from chm^{35} identified a frameshift mutation early in the laminin I domain predicted to cause truncation of nearly half the protein (Fig. 3K,L). The tight genetic linkage, expression pattern, reduced expression in *chm*, morpholino phenocopy and definitive frameshift mutation in chm^{35} all support the conclusion that the two alleles of *chm* both have lesions in the *Cs*-lamα3/4/5 gene.

Cs-lamα3/4/5 protein is localized to perinotochordal surfaces

Given the *chm* phenotype, we hypothesized that *Cs*-lamα3/4/5 might be a component of a perinotochordal ECM. Perinotochordal basement membranes have been described in the mature notochords of many species, where they are thought to form an inelastic sheath that opposes the turgor pressure generated by vacuolization (Stemple, 2005). Earlier developmental roles for perinotochordal ECM molecules are not as well established. Perinotochordal ECM has been observed in *Ciona* embryos by electron microscopy as early as tailbud stage, but does not form a thick, multilayered basement membrane until much later, during vacuolization (Cloney, 1964). Although the molecular composition of the ascidian perinotochordal ECM is unknown, laminins are known to be important components of the zebrafish perinotochordal basement membrane (Scott and Stemple, 2005).

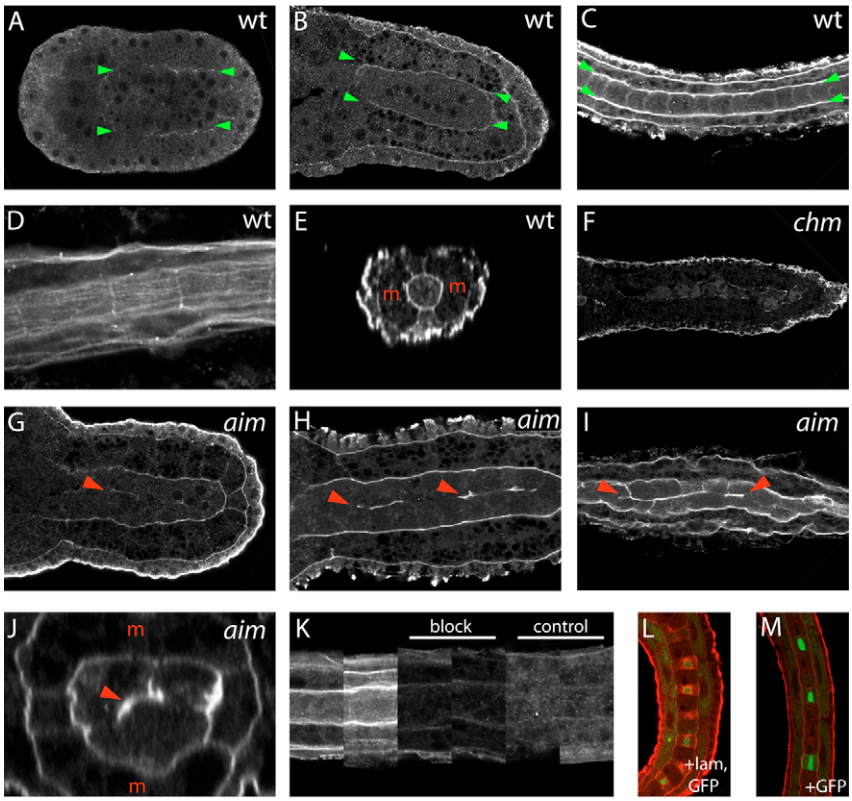

Fig. 4. Immunolocalization of *Cs*-lamα3/4/5. (**A-C**) Single confocal sections through the notochords of wild-type ascidian embryos stained for *Cs*-lamα3/4/5 at (A) late neurula, (B) early tailbud and (C) late tail stages. Anterior is to the left. Green arrowheads indicate the lateral edges of the notochord or notochord primordium. (**D**) Tangential section grazing the perinotochordal surface of a wild-type late-tail-stage embryo. (**E**) Reconstructed *z*-section across the notochord of a mid-tail wild-type embryo. Red 'm's indicate the lateral blocks of muscle cells. (**F**) Single confocal section through the notochord of a mid-tail-stage *chm/chm* embryo. (**G-I**) Single confocal sections through the notochords of (G) mid-tail, (H) mid-late tail and (I) late tail stage *aim/aim* embryos. Red arrowheads show ectopic laminin localization on intranotochordal cell surfaces. (**J**) Reconstructed *z*-section across the notochord of an *aim/aim* mid-late-tail-stage embryo. Red 'm's indicate the lateral blocks of muscle cells, and the red arrowhead shows ectopic laminin. (**K**) Representative images from multiple wild-type embryos stained under standard conditions with the *Cs*-lamα3/4/5 antibody, the *Cs*-lamα3/4/5 antibody blocked by prebinding to *Cs*-lamα3/4/5 peptide, or with control non-immune normal rabbit serum. (**L**,**M**) *Cs*-lamα3/4/5 antibody staining (red) and GFP staining (green) in *C. intestinalis* embryos electroporated with (L) notochord-specific expression plasmids for both *Cs*-lamα3/4/5 and GFP, or (M) GFP plasmid alone.

We raised a rabbit polyclonal antibody against a bacterially expressed segment of *Cs*-lamα3/4/5 that is not conserved in the second *C. savignyi* alpha laminin gene. Staining was first evident at neurula stage as a faint, irregular outline around the outside of the notochord primordium (Fig. 4A). By early tailbud stage there was robust staining around the notochord primordium as well as expression between the epidermis and the underlying tissues (Fig. 4B). By late tail extension stage the perinotochordal staining was stronger yet (Fig. 4C). In tangential optical sections, longitudinal fibers could be seen along the notochord surface (Fig. 4D). In reconstructed z-sections, the strongest staining was around the notochord, but it also demarcated all of the major tissues in the tail: notochord, muscle, epidermis, nerve cord and endodermal strand (Fig. 4E). There was also peripheral epidermal staining that was somewhat variable dependent on the proteinase treatment necessary to unmask the laminin epitope.

In *chm* embryos, staining was still evident but noticeably decreased. The perinotochordal staining in particular was weak and patchy (Fig. 4F). As further controls for antibody specificity, preblocking the antibody with recombinant antigen greatly decreased the observed staining, and little to no staining was seen in embryos stained with non-immune rabbit serum (Fig. 4K). Mosaic overexpression of full-length *Cs*-lamα3/4/5 by electroporation also gave rise to increased staining in the expressing cells (Fig. 4L,M). We conclude that the antibody is a faithful probe for *Cs*-lamα3/4/5 protein localization and that the perinotochordal staining observed is fully consistent with a role as a perinotochordal basement membrane component involved in notochord boundary formation. The subectodermal staining is also consistent with the epidermal tail protrusion phenotype, which may involve decreased adhesion between the ectoderm and underlying tissues.

Cs-lamα3/4/5 polarity is perturbed in the PCP mutant *aim*

To examine potential interactions between the PCP pathway and laminin-mediated boundary formation, we stained *aim* embryos with the *Cs*-lamα3/4/5 antibody. The perinotochordal staining remained robust, but we also observed large patches of staining deep within the notochord, between adjacent cells (Fig. 4G-J). This internal laminin expression was typically quite mild at early stages and became progressively more severe over time, suggesting that PCP signaling is involved in maintenance rather than establishment of *Cs*-lamα3/4/5 polarization.

Laminin-mediated boundary formation can drive considerable tail elongation in the absence of PCP signaling

The observation of ectopic intranotochordal laminin in *aim* embryos caused us to reconsider aspects of the *aim* phenotype. It was previously shown that *aim* notochord cells have a near-complete loss of the mediolateral bias in actin-rich cell protrusions thought to drive intercalation (Jiang et al., 2005; Munro and Odell, 2002b). Such measurements were made, however, only very early in the process of intercalation, and the *aim* notochord does continue to intercalate, albeit very slowly, such that it eventually becomes approximately two cells wide.

In Fig. 5A,B, we compare an early-tailbud-stage wild-type embryo with a considerably (~2 hours) older *aim* embryo, in order to compare embryos at a similar degree of intercalation. (A wild-type embryo of identical age to Fig. 5B has already completed intercalation, as shown in Fig. 1D,F.) Although they had notochords of roughly comparable length and width, the *aim* notochord cells were less mediolaterally elongated than in wild type, and they failed to polarize their nuclei away from the notochord boundary. Despite

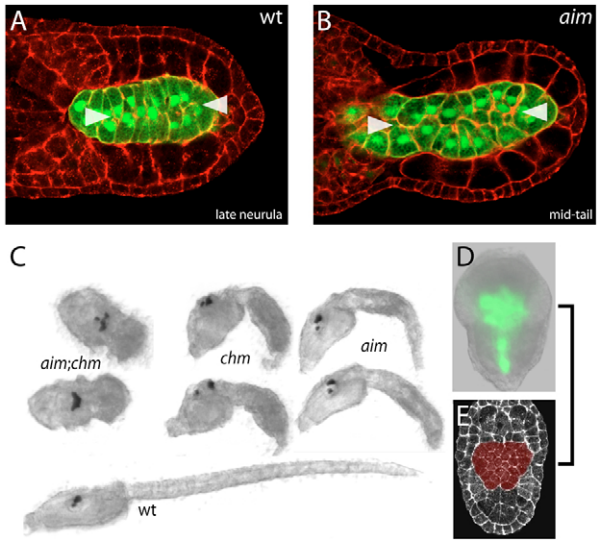

Fig. 5. *Cs*-lamα3/4/5 can drive considerable tail extension in the absence of a functional PCP pathway in *C. savignyi*. (**A**,**B**) Confocal section through (A) late neurula stage wild-type embryo and (B) mid-tail-stage *aim/aim* embryo. Anterior to the left. *bra:GFP* in green, phallacidin in red. White arrowheads indicate medially polarized actin-rich structures. (**C**) Brightfield images of hatched larvae of the indicated genotypes. (**D**) Widefield *bra:GFP* fluorescence in an *aim/aim*;*chm/chm* embryo. Wild-type sibs (not shown) are at late tailbud stage. (**E**) Neurula-stage wild-type embryo, with phallacidin staining in white and the notochord primordium pseudocolored in red.

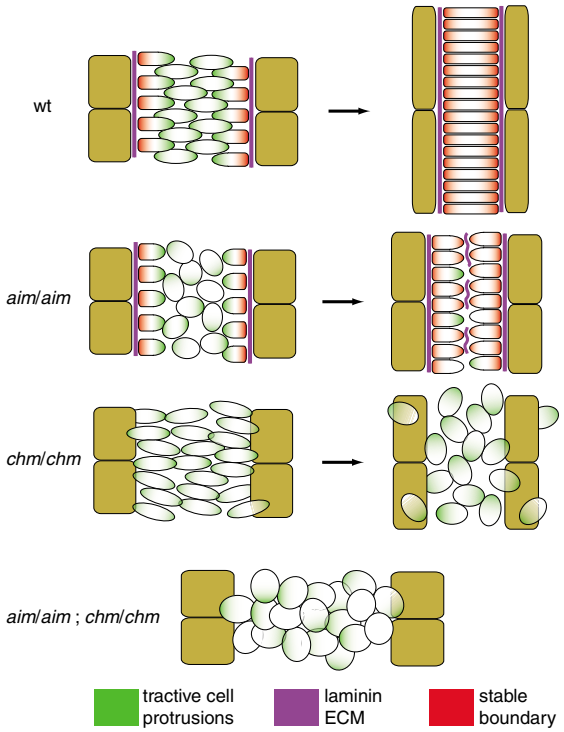

Fig. 6. A model of ascidian notochord morphogenesis. In wild-type embryos, the PCP pathway mediates mediolateral intercalation behavior and a perinotochordal laminin-containing ECM mediates boundary formation. When the PCP pathway is disrupted in *aim/aim* embryos, mediolaterally-biased notochord cell intercalation is perturbed but considerable convergence and extension still slowly occur. This may be the result of randomly moving notochord cells being 'trapped' where they stochastically contact the notochord boundary. The PCP pathway is also required to maintain perinotochordal/intranotochordal *Cs*-lamα3/4/5 polarity. The failure of *aim/aim* notochord cells to complete the final stages of intercalation may reflect this deposition of laminin on intranotochordal surfaces. In *chm/chm* embryos there is a defect in perinotochordal boundary formation and notochord cells become dispersed in the tail. Despite this morphogenetic defect, there is still a moderate degree of convergence and extension, which is probably due to the PCP pathway given that the *aim/aim*;*chm/chm* double mutant shows a near complete failure in convergence and extension. Although the lack of epistasis suggests that the two processes act at least partly in parallel, the true relationship is clearly complex, given the role of *aim* in maintaining *Cs*-lamα3/4/5 polarity and the role of *Cs*-lamα3/4/5 in maintaining polarized cell behaviors. wt, wild type.

these differences, the *aim* notochord cells were, in many respects, relatively normal: they formed a neat, flat edge with the flanking muscle cells; they showed a degree of mediolateral elongation; and they typically showed concentrations of actin on medial cell surfaces opposite the notochord boundary and not on their anterior and posterior edges (white arrowheads in Fig. 5B).

We hypothesized that the considerable degree of notochord morphogenesis in *aim* might be the result of *Cs*-lamα3/4/5-mediated boundary formation, given that *aim* embryos form a smooth and compact notochord boundary. To test this hypothesis, we constructed the *aim*/*aim*;*chm*/*chm* double mutant. Unlike either single mutant, the double mutant showed essentially no tail extension (Fig. 5C), but still had the normal number of *brachyury*-expressing notochord cells (Fig. 5D and data not shown; for molecular genotyping of these phenotypic classes, see Fig. S3 in the supplementary material). With the exception of a small number of notochord cells that migrated between the two blocks of muscle cells (probably the secondary notochord lineage), the majority of notochord cells remained in an isodiametric group comparable to the wild-type notochord primordium before the onset of intercalation (compare Fig. 5D with 5E). Having shown that laminin-mediated boundary formation is sufficient to drive considerable tail elongation in the absence of PCP signaling, one question that remains is why *aim* embryos fail to complete intercalation, given that they do slowly develop polarized cell morphologies. We suggest that this may reflect the observed failure to maintain the perinotochordal/intranotochordal polarity of ECM proteins such as laminin, giving rise to an ectopic basement membrane on intranotochordal surfaces and preventing further intercalation. See Fig. 6 for a diagram of this model.

DISCUSSION

Importance of the perinotochordal boundary

Although not well understood on a cellular or molecular level, there is considerable evidence that the notochord boundary is of great importance in shaping the converging and extending mesoderm. Keller and colleagues initially described how intercalating *Xenopus* mesoderm cells are 'captured' such that they become quiescent on cell surfaces contacting the notochord/somite boundary (Keller et al., 1989; Shih and Keller, 1992a). In ascidian embryos, Munro and Odell used explant and ablation studies to demonstrate that the notochord primordium requires certain contacts with neighboring tissues in order to converge and extend (Munro and Odell, 2002a). Ascidian tail extension can also be perturbed by misexpression of a Snail-VP16 construct that gives rise to notochord fate in a subset of

muscle cells, suggesting that the orderly physical arrangement of the notochord/muscle boundary is essential (Fujiwara et al., 1998). Here we have shown that the ascidian notochord boundary supports several complex behaviors: a dynamic spreading behavior as notochord cell surfaces are captured by the boundary; shearing along the boundary between the notochord and muscle cells; rhythmic pulsatile movements after intercalation is complete; and, most significantly, considerable convergence and extension of the notochord, even in the absence of a functional PCP pathway.

While numerous genetic, pharmacological and embryological approaches have been used to study notochord development in many model systems, the severe phenotype seen in *chm* has not been described in other contexts. In *Xenopus* embryos, perturbations of perinotochordal ECM molecules such as fibrillin and fibronectin cause convergent extension phenotypes that may reflect defects in boundary capture, but do not cause a wholesale disruption of the notochord boundary as seen in *chm* (Davidson et al., 2006; Skoglund and Keller, 2006). We suggest that laminins be considered candidate vertebrate boundary capture signals.

The 3D tissue architecture of the converging and extending ascidian notochord is quite complex. As it narrows and lengthens, it not only intercalates but also undergoes a ventrally-oriented invagination movement that transforms it from a sheet to a rod (Munro and Odell, 2002b). Although it is clear that morphogenetic processes at the notochord boundary are of great importance in shaping the ascidian notochord, it is not clear if there is a morphologically distinct population of border cells. It is possible that all notochord cells are, at some dorsoventral position, in partial contact with the nascent perinotochordal boundary from the earliest stages, and that what is presented in Fig. 6 as cells being trapped de novo by the boundary actually represents cells expanding the fraction of their periphery in contact with the boundary. Competition for an initially limiting expanse of bounding surfaces may help explain the extreme length-to-width ratios (Munro and Odell, 2002b) of the disk-shaped cells in the just-intercalated notochord.

Laminins in notochord morphogenesis

Although it is possible that a specific role for laminin in notochord boundary formation is unique to the ascidians, we argue that the novelty of the *chm* phenotype is likely to reflect the morphological simplicity of the ascidian embryo and the genomic simplicity of its complement of ECM components. In vertebrates, for example, there are typically five alpha, four beta and three gamma laminin subunits (Li et al., 2003), as opposed to two alpha, one beta and one gamma in ascidians (Sasakura et al., 2003). Analysis of the large set of murine laminins has been complicated by essential early roles in preimplantation development in addition to considerable redundancy and compensation between various family members (Li et al., 2003). Laminins are clearly important for vertebrate notochord development, as indicated by the zebrafish mutations *bashful* (lamα1), *grumpy* (lamβ1) and *sleepy* (lamγ1), which have later roles in notochord differentiation (Parsons et al., 2002; Pollard et al., 2006). While *grumpy* and *sleepy* mutants show a nearly complete absence of reactivity to a mouse laminin-1 antibody (Parsons et al., 2002), it is likely that there is still considerable functional redundancy between the zebrafish laminins that may mask a more *chm*-like phenotype. For example, injection of lamα5 morpholino into *bashful* causes a severe disruption of notochord and other tissues that has not been characterized in detail (Pollard et al., 2006). A convergent extension phenotype has also been seen in zebrafish embryos depleted of a galactosyl-transferase important in post-translational modifications of laminin (Machingo et al., 2006).

PCP signaling and the ECM

Recent work suggests that there may be important interactions between vertebrate PCP signaling and the extracellular matrix. The PCP proteins Prickle, Strabismus and Dishevelled have been shown to be important in restricting fibronectin protein localization to the outer surfaces of the *Xenopus* notochord (Goto et al., 2005), similar to what we observe with laminin localization in the *Cs*-pk mutation *aim*. Tissue separation defects have also been described in *Xenopus* and zebrafish embryos with perturbed non-canonical Wnt/PCP signaling (Ulrich et al., 2003; Winklbauer et al., 2001). It may be of considerable interest to look for defects in polarized ECM deposition in zebrafish PCP mutants and other contexts that have previously been interpreted strictly in terms of perturbed cell motility.

Interactions between PCP signaling and laminin-mediated boundary formation

Unlike in *aim* mutants, early notochord intercalation in *chm* is relatively normal and then becomes progressively more aberrant, suggesting that one role of the notochord boundary is to maintain polarized cell behaviors initiated by PCP signaling. *Cs*-lamα3/4/5-mediated boundary formation is able, however, to cause considerable narrowing and lengthening of the notochord even in the absence of a functional PCP pathway, as indicated by the near-complete loss of convergence and extension in the *aim*/*aim*;*chm*/*chm* double mutant compared with *aim*/*aim*. As prickle and *Cs*-lamα3/4/5 are predominantly expressed in the notochord, the severity of this phenotype suggests that the ascidian muscle and neural plate do not have a strong ability to autonomously converge and extend as seen in vertebrates.

Although the double mutant phenotype indicates that *aim* and *chm* act largely in parallel, the observation of intranotochordal laminin in *aim* embryos suggests that there is a more complex relationship. As this intranotochordal staining is initially minimal and becomes progressively stronger over time, it appears that PCP signaling is involved in the maintenance rather than the initial establishment of perinotochordal ECM polarity. The *aim* mutation truncates much of the *Cs*-Pk protein, causes a complete loss of membrane localization of the PCP effector molecule Dishevelled, and shows no maternal effect (Jiang et al., 2005), so the *aim* phenotype probably reflects a complete loss of Pk function. We cannot fully exclude, however, that there may be residual function in *chm* or *aim* that might confound epistasis analysis. It will be of great interest to determine whether perinotochordal laminin localization involves polarized secretion, stabilization or degradation, and how later perinotochordal/intranotochordal polarity relates to earlier mediolateral polarity. We suggest that PCP signaling has multiple distinct functions in ascidian notochord morphogenesis, including an early role in the mediolateral polarity of tractive cell protrusions (Jiang et al., 2005), a subsequent role in maintaining polarized ECM localization (this study), a role in polarizing cell nuclei away from the boundary late in intercalation (this study), and a role in anteroposterior polarity after intercalation is complete (Jiang et al., 2005). Advanced imaging methods will probably be of great importance in supporting and extending these models of notochord morphogenesis.

We thank Matt Kourakis and Wendy Reeves for helpful comments on the manuscript and William Graham and Hank Hymanson for their assistance in identifying carriers. This work was supported by NIH grants HD038701 and GM075049 to W.C.S. and a Santa Barbara Foundation/Tri-County Blood Bank Fellowship to M.T.V.

Supplementary material

Supplementary material for this article is available at http://dev.biologists.org/cgi/content/full/135/1/33/DC1

References

Arenas-Mena, C., Cameron, A. R. and Davidson, E. H. (2000). Spatial expression of Hox cluster genes in the ontogeny of a sea urchin. *Development* **127**, 4631-4643.

Berrill, N. J. (1930). Studies in tunicate development. Part I. General physiology of development of simple Ascidians. *Philos. Trans. R. Soc. Lond. B Biol. Sci.* **218**, 37-78.

Cloney, R. A. (1964). Development of the ascidian notochord. *Acta Embryol. Morphol. Exp.* **7**, 111-130.

Corbo, J. C., Levine, M. and Zeller, R. W. (1997). Characterization of a notochord-specific enhancer from the Brachyury promoter region of the ascidian, *Ciona intestinalis*. *Development* **124**, 589-602.

Davidson, L. A., Marsden, M., Keller, R. and Desimone, D. W. (2006). Integrin alpha5beta1 and fibronectin regulate polarized cell protrusions required for *Xenopus* convergence and extension. *Curr. Biol.* **16**, 833-844.

Deschet, K., Nakatani, Y. and Smith, W. C. (2003). Generation of Ci-Brachyury-GFP stable transgenic lines in the ascidian *Ciona savignyi*. *Genesis* **35**, 248-259.

Fujiwara, S., Corbo, J. C. and Levine, M. (1998). The snail repressor establishes a muscle/notochord boundary in the *Ciona* embryo. *Development* **125**, 2511-2520.

Goto, T., Davidson, L., Asashima, M. and Keller, R. (2005). Planar cell polarity genes regulate polarized extracellular matrix deposition during frog gastrulation. *Curr. Biol.* **15**, 787-793.

Hendrickson, C., Christiaen, L., Deschet, K., Jiang, D., Joly, J. S., Legendre, L., Nakatani, Y., Tresser, J. and Smith, W. C. (2004). Culture of adult ascidians and ascidian genetics. *Methods Cell Biol.* **74**, 143-170.

Hotta, K., Takahashi, H., Erives, A., Levine, M. and Satoh, N. (1999). Temporal expression patterns of 39 Brachyury-downstream genes associated with notochord formation in the *Ciona intestinalis* embryo. *Dev. Growth Differ.* **41**, 657-664.

Hotta, K., Takahashi, H., Asakura, T., Saitoh, B., Takatori, N., Satou, Y. and Satoh, N. (2000). Characterization of Brachyury-downstream notochord genes in the *Ciona intestinalis* embryo. *Dev. Biol.* **224**, 69-80.

Imai, K. S., Satou, Y. and Satoh, N. (2002). Multiple functions of a Zic-like gene in the differentiation of notochord, central nervous system and muscle in *Ciona savignyi* embryos. *Development* **129**, 2723-2732.

Imai, K. S., Hino, K., Yagi, K., Satoh, N. and Satou, Y. (2004). Gene expression profiles of transcription factors and signaling molecules in the ascidian embryo: towards a comprehensive understanding of gene networks. *Development* **131**, 4047-4058.

Jiang, D., Munro, E. M. and Smith, W. C. (2005). Ascidian prickle regulates both mediolateral and anterior-posterior cell polarity of notochord cells. *Curr. Biol.* **15**, 79-85.

Keller, R. (2002). Shaping the vertebrate body plan by polarized embryonic cell movements. *Science* **298**, 1950-1954.

Keller, R., Cooper, M. S., Danilchik, M., Tibbetts, P. and Wilson, P. A. (1989). Cell intercalation during notochord development in *Xenopus laevis*. *J. Exp. Zool.* **251**, 134-154.

Kirkpatrick, P. and d'Ardenne, A. J. (1984). Effects of fixation and enzymatic digestion on the immunohistochemical demonstration of laminin and fibronectin in paraffin embedded tissue. *J. Clin. Pathol.* **37**, 639-644.

Li, S., Edgar, D., Fassler, R., Wadsworth, W. and Yurchenco, P. D. (2003). The role of laminin in embryonic cell polarization and tissue organization. *Dev. Cell* **4**, 613-624.

Machingo, Q. J., Fritz, A. and Shur, B. D. (2006). A beta1,4-galactosyltransferase is required for convergent extension movements in zebrafish. *Dev. Biol.* **297**, 471-482.

Marsden, M. and DeSimone, D. W. (2006). Integrin-ECM interactions regulate cadherin-dependent cell adhesion and are required for convergent extension in *Xenopus*. *Curr. Biol.* **13**, 1182-1191.

Miyamoto, D. M. and Crowther, R. J. (1985). Formation of the notochord in living ascidian embryos. *J. Embryol. Exp. Morphol.* **86**, 1-17.

Munro, E. M. and Odell, G. (2002a). Morphogenetic pattern formation during ascidian notochord formation is regulative and highly robust. *Development* **129**, 1-12.

Munro, E. M. and Odell, G. M. (2002b). Polarized basolateral cell motility underlies invagination and convergent extension of the ascidian notochord. *Development* **129**, 13-24.

Munro, E., Robin, F. and Lemaire, P. (2006). Cellular morphogenesis in ascidians: how to shape a simple tadpole. *Curr. Opin. Genet. Dev.* **16**, 399-405.

Nakatani, Y., Moody, R. and Smith, W. C. (1999). Mutations affecting tail and notochord development in the ascidian *Ciona savignyi*. *Development* **126**, 3293-3301.

Parsons, M. J., Pollard, S. M., Saude, L., Feldman, B., Coutinho, P., Hirst, E. M. and Stemple, D. L. (2002). Zebrafish mutants identify an essential role for laminins in notochord formation. *Development* **129**, 3137-3146.

Pollard, S. M., Parsons, M. J., Kamei, M., Kettleborough, R. N., Thomas, K. A., Pham, V. N., Bae, M. K., Scott, A., Weinstein, B. M. and Stemple, D. L. (2006). Essential and overlapping roles for laminin alpha chains in notochord and blood vessel formation. *Dev. Biol.* **289**, 64-76.

Reintsch, W. E., Habring-Mueller, A., Wang, R. W., Schohl, A. and Fagotto, F. (2005). Beta-catenin controls cell sorting at the notochord-somite boundary independently of cadherin-mediated adhesion. *J. Cell Biol.* **170**, 675-686.

Sasaki, T., Fassler, R. and Hohenester, E. (2004). Laminin: the crux of basement membrane assembly. *J. Cell Biol.* **164**, 959-963.

Sasakura, Y., Shoguchi, E., Takatori, N., Wada, S., Meinertzhagen, I. A., Satou, Y. and Satoh, N. (2003). A genomewide survey of developmentally relevant genes in *Ciona intestinalis*. X. Genes for cell junctions and extracellular matrix. *Dev. Genes Evol.* **213**, 303-313.

Scott, A. and Stemple, D. L. (2005). Zebrafish notochordal basement membrane: signaling and structure. *Curr. Top. Dev. Biol.* **65**, 229-253.

Shih, J. and Keller, R. (1992a). Cell motility driving mediolateral intercalation in explants of *Xenopus laevis*. *Development* **116**, 901-914.

Shih, J. and Keller, R. (1992b). Patterns of cell motility in the organizer and dorsal mesoderm of Xenopus laevis. *Development* **116**, 915-930.

Skoglund, P. and Keller, R. (2006). *Xenopus* fibrillin regulates directed convergence and extension. *Dev. Biol.* **301**, 404-416.

Stemple, D. L. (2005). Structure and function of the notochord: an essential organ for chordate development. *Development* **132**, 2503-2512.

Ulrich, F., Concha, M. L., Heid, P. J., Voss, E., Witzel, S., Roehl, H., Tada, M., Wilson, S. W., Adams, R. J., Soll, D. R. et al. (2003). Slb/Wnt11 controls hypoblast cell migration and morphogenesis at the onset of zebrafish gastrulation. *Development* **130**, 5375-5384.

Veeman, M. T., Axelrod, J. D. and Moon, R. T. (2003). A second canon. Functions and mechanisms of beta-catenin-independent Wnt signaling. *Dev. Cell* **5**, 367-377.

Wallingford, J. B., Fraser, S. E. and Harland, R. M. (2002). Convergent extension: the molecular control of polarized cell movement during embryonic development. *Dev. Cell* **2**, 695-706.

Wang, Y. and Nathans, J. (2007). Tissue/planar cell polarity in vertebrates: new insights and new questions. *Development* **134**, 647-658.

Winklbauer, R., Medina, A., Swain, R. K. and Steinbeisser, H. (2001). Frizzled-7 signalling controls tissue separation during *Xenopus* gastrulation. *Nature* **413**, 856-860.